Chapter 5
Interactions of Biomaterial Surfaces with Proteins and Cells

Zhonglin Lyu, Yi Zou, Qian Yu, and Hong Chen

Abstract The interactions of material surfaces with proteins and cells play a vital role in various biological phenomena and determine the ultimate biofunctionality of a given material in contact with a given biological environment. In this chapter, we used the gold nanoparticle layer (GNPL) with three-dimensional micro- and nano-sized structures as an example to discuss the interactions of material surfaces with proteins and cells. GNPL is deposited onto a variety of substrates such as gold surface and enzyme-linked immunosorbent assay (ELISA) plate; the amount and activity of the absorbed proteins, as well as cell behaviors including attachment, proliferation, and differentiation on GNPL-modified surfaces, are systematically investigated. In addition, the synthetic effects of surface topography and surface chemistry are also studied. The results show that GNPL improves protein adsorption, favors the maintenance of their conformation and bioactivity, and further enhances cell adhesion. After modification with protein-resistant polymers and specific ligands, GNPL selectively binds certain proteins and cells from protein and cell mixtures, including the highly complex environment of serum. Moreover, under laser irradiation, GNPL shows the ability for the delivery of various macromolecules to different cell types (including hard-to-transfect cell types) and the ability for high-efficiency eradication of pathogenic bacteria. It is concluded that GNPLs hold great promise in many biomedical fields such as protein detection, regulation of cell behaviors, capture of circulating cancer cells, macromolecular delivery to living cells, and antibacterial application.

Keywords Gold nanoparticle layer · Topography · Surface modification · Protein adsorption · Cell behavior · Antibacterial application

Z. Lyu · Y. Zou · Q. Yu · H. Chen (✉)
State and Local Joint Engineering Laboratory for Novel Functional Polymeric Materials, College of Chemistry, Chemical Engineering and Materials Science, Soochow University, Suzhou, China
e-mail: chenh@suda.edu.cn

C. Gao (ed.), *Polymeric Biomaterials for Tissue Regeneration*,
https://doi.org/10.1007/978-981-99-6948-7_5

The interactions of material surfaces with proteins and cells play a vital role in various biological phenomena and determine the ultimate biofunctionality of a given material in contact with a given biological environment [1]. The effects of surface topography and roughness (especially at the nanometer scale) on protein and cell behavior have attracted increasing attention since topographic features may have dimensions similar to those of proteins and cell membrane receptors [2–4]. For example, gold nanoparticle layers (GNPLs) consist of nanoparticle aggregates with a distribution of sizes and three-dimensional micro- and nano-sized porous structures [5–11]. GNPLs hold great promise in biomedical applications, for example, biosensors and tissue engineering, due to their large surface-to-volume ratio, efficient electron transfer, good stability, and high loading capacity [8, 12, 13]. Formation of GNPL on material surfaces is usually achieved by reduction of tetrachloroauric (III) acid either through surface-bonded reducing groups or reducing agents [5, 6, 12, 14]. For example, Zhang and coworkers used the Si-H reducing group in the residual curing agent (silicone resin solution) in poly(dimethylsiloxane) (PDMS) matrix to reduce $HAuCl_4$ in the preparation of a PDMS–gold nanoparticle composite film. Wang and coworkers have also reported a method for fabricating PDMS-GNPs films [12]. In another report, chitosan, used as a reducing and stabilizing agent, was coated on PDMS; the coated PDMS was then immersed in $HAuCl_4$ solution to form a layer of GNPs [14]. In our research, stable GNPL were prepared on a variety of materials via a facile and low-cost glucose reduction method [5, 6]. The applications of GNPL for control of protein adsorption and regulation of cell behavior are discussed in the following sections.

5.1 Control of Protein Adsorption

The interaction of biomaterials with proteins is of crucial importance in various applications including biochips [15], biosensors [16], medical device coatings [17], and drug delivery [18]. Controlling the adsorption of proteins (e.g., antibodies, enzymes) on material surfaces and conserving their activity are essential in the design of functional surfaces [19]. In this section, protein adsorption on GNPL-modified enzyme-linked immunosorbent assay (ELISA) plates is discussed in detail. The combined effects of the micro-/nanostructures of the GNPL and the chemistry of polymer brushes grafted on GNPL on protein adsorption are highlighted. The modification of GNPL with pH-responsive polymers for controllable capture and release of proteins is also explored in this discussion.

5.1.1 Protein Adsorption on GNPL-Modified ELISA Plates

ELISA is widely used in clinical diagnosis due to its relative simplicity, low cost, and high sensitivity [20, 21]. A major limitation is low binding affinity of antigens

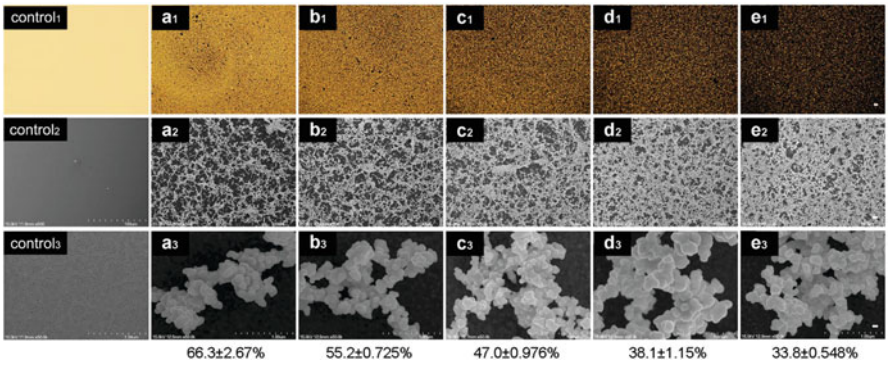

Fig. 5.1 Characterization of unmodified (control) and GNPL-modified ELISA plates. The volumes of plating solution for GNPL (**a**–**e**) were 50, 100, 150, 200, and 250 μL, respectively. (**a1**–**e1**) are visible light micrographs (bar: 100 μm); (**a2**–**e2**) are field emission scanning electron microscopy (FESEM) images (*bar*: 10 μm); (**a3**–**e3**) are high-magnification FESEM images (*bar*: 100 nm); the numbers under the columns are the respective porosity values for GNPL (**a**–**e**). (Reprinted from Ref. [5] with permission. Copyright 2011 American Chemical Society)

and antibodies; in addition, the accessibility of adsorbed proteins on a standard "two-dimensional" microplate surface for the recognition and binding of antigens and antibodies may be limited [22]. To improve accessibility and sensitivity, we have investigated modification of ELISA plates with GNPL to give surfaces that may be described as "three dimensional" [5].

GNPL exhibits three-dimensional porous structures that are composed of gold nanoparticle aggregates with thickness in the micrometer range. By adjusting the volume of the plating solution in the wells, a series of GNPLs with different porosity rates were obtained. With increasing solution volume, the micro- and nano-sized porous structures became more densely aggregated and the porosity value decreased gradually (Fig. 5.1) [5]. It was found that the quantity of proteins (lysozyme (LYZ), human serum albumin (HSA), and fibrinogen (Fg), used as model proteins of different size) adsorbed on GNPL-modified ELISA plates increased significantly with increasing solution volume; e.g., for GNPL prepared with the highest solution volume, the adsorbed quantities of LYZ, HSA, and Fg were, respectively, 2.76-, 2.34-, and 3.26-fold higher than on the unmodified plate. Moreover, due to the micro- and nanostructures of the GNPL, the activity of LYZ absorbed on GNPL was found to be at least 2.65-fold higher than on the unmodified plate. The GNPL-modified plate was shown to amplify the ELISA signals for carcinoembryonic antigen (CEA) and antithrombin (AT) and to increase the limits of detection (LOD) of these antigens significantly. Useful ELISA signals were obtained on GNPL-modified plates when the quantity of CEA was above 2 ng/well; in contrast, no useful signal was obtained on the pristine high-binding ELISA plate even for quantities greater than 10 ng/well. The LOD for AT in buffer solution with GNPL-modified plate was two orders of magnitude lower than for the unmodified plate.

To overcome the limitation of indirect ELISA to selectively bind a specific target from a multiprotein fluid such as serum or plasma, we proposed a GNPL-based ELISA in sandwich format [6]. Sandwich ELISA is widely used in various commercially available kits. In "traditional" sandwich ELISA, the captured (adsorbed) antibody (Ab) binds to the ELISA plate by physical adsorption, resulting in random orientation of the Ab molecules and thus in decreased performance. We hypothesized that an optimum orientation of Ab on the ELISA plate by covalent attachment might improve performance [23]. Accordingly, we immobilized goat anti-rabbit IgG (IgG-alkaline phosphatase (ALP)) on GNPL using 1-ethyl-3-(3-dimethylaminopropyl) carbodiimide hydrochloride (EDC)/*N*-hydroxysuccinimide (NHS) conjugation chemistry. We showed that the activity of IgG covalently immobilized on the GNPL plate was 61% higher than that of IgG physically adsorbed on the unmodified plate.

This result may be attributed, in part, to the improved binding efficiency of the GNPL-modified, compared to the unmodified, ELISA plate; more importantly, the GNPL-modified plate may favor an Ab orientation that facilitates the binding of the IgG substrate to the enzyme. The GNPL-modified ELISA plate showed a lower LOD and higher sensitivity for rabbit IgG in buffer and CEA in plasma. For IgG in buffer, the detection limit of the GNPL-modified ELISA was 0.0512 ng/mL, two orders of magnitude lower than that of the unmodified plate (1.28 ng/mL). For CEA in plasma, the GNPL-modified plate gave a stronger ELISA signal than the unmodified, high-binding ELISA plate as indicated by the deeper color. This was especially true for CEA concentrations greater than 8 ng/mL. The LOD for the GNPL-modified ELISA plate was 2 ng/mL compared to 4 ng/mL for a typical commercial ELISA kit (Linc-Bio Co.).

5.1.2 Controlling Protein Adsorption on GNPL Modified with Hydrophilic Polymer Brushes

Surfaces with micro-/nanostructures adsorb greater quantities of protein than smooth surfaces on a nominal area basis. On the other hand, surfaces modified with hydrophilic polymers such as poly[oligo(ethylene glycol) methacrylate] (POEGMA) tend to resist nonspecific protein adsorption [7, 9]. It was of interest, therefore, to investigate the combined effects of micro-/nanostructures and hydrophilic polymers on protein adsorption. GNPL were modified with POEGMA by surface-initiated atom transfer radical polymerization (SI-ATRP) [7, 9]. Protein adsorption was measured using radiolabeled protein. It was found for human serum albumin (HSA, one of the most abundant proteins in the body) that adsorption on the GNPL surface was about 5.8-fold higher than on smooth Au (sAu) (Fig. 5.2). After modification with POEGMA, adsorption was reduced by about 97%. Adsorption on GNPL-POEGMA and sAu-POEGMA was similar (Fig. 5.2) indicating the strong protein resistance of POEGMA.

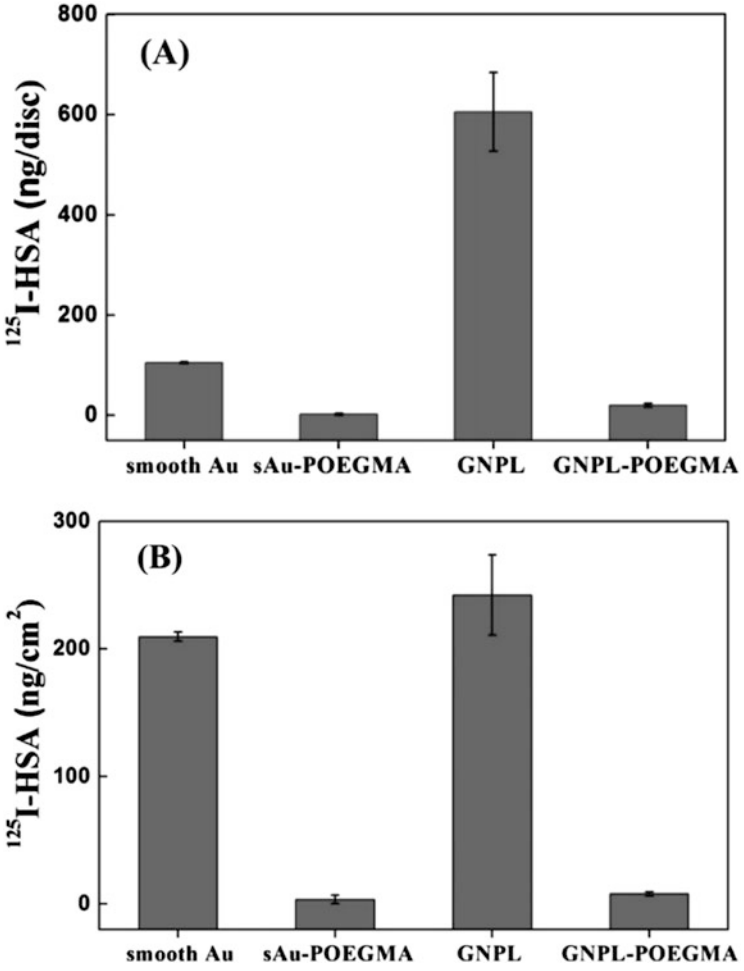

Fig. 5.2 The adsorption of 1 mg/mL HSA measured using ^{125}I radiolabeling method, as expressed in (**a**) nanograms/disc or (**b**) nanograms/cm^2. Data are means ± SD ($n = 3$). (Reprinted from Ref. [9] with permission. Copyright 2012 American Chemical Society)

5.1.3 Capture and Release of Proteins on Multifunctional GNPL

In recent years, various functional surfaces modified with different functional proteins have emerged as novel and active biomaterials due to their numerous applications such as disease therapy, molecular diagnostics, and tissue engineering [24–26]. For these surfaces, to achieve tunable surface bioactivity is vital. An ideal multifunctional surface of this kind should be able to highly regulate the amount of proteins adsorbed on and released from the surface. It should also be able to

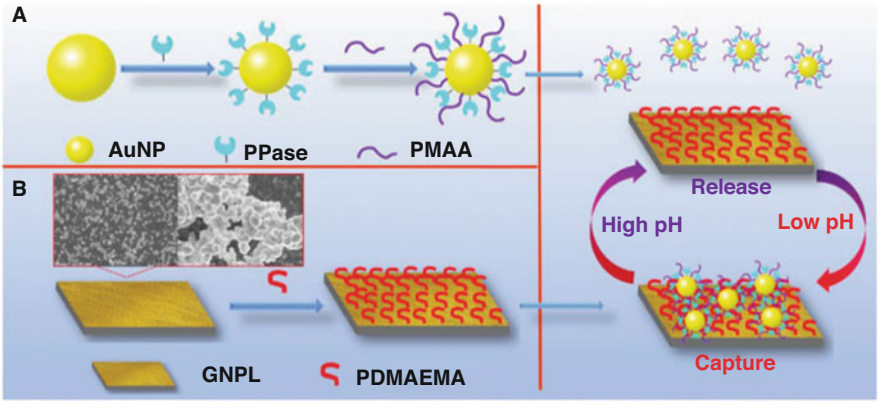

Fig. 5.3 Synthesis of (**a**) AuNP-PPase-PMAA conjugates and (**b**) GNPL-PDMAEMA surfaces; the reversible capture/release of AuNP-PPase-PMAA conjugates on GNPL-PDMAEMA surfaces at different pH values is shown in (**c**). (Reprinted from Ref. [27] with permission. Copyright 2017 Royal Society of Chemistry)

regulate the available bioactivity of the surface. To develop such a multifunctional system, we used pH-sensitive polymers, gold nanoparticles (AuNPs), and GNPLs [27]. pH-sensitive polymers have been proven efficient in responding in real time to pH changes through regulating their chemical and physical properties to achieve protein capture and release [28, 29]. AuNPs and GNPLs were used to introduce nanostructures to the system with the goal to increase the amount of proteins that can be modulated. In detail, this novel system contains (1) AuNPs comodified with an enzyme and poly(methacrylic acid) (PMAA), e.g., AuNP-pyrophosphatase (PPase)-PMAA, as nanostructured protein carriers; (2) GNPLs modified with poly (2-(dimethylamino)ethyl methacrylate) (PDMAEMA), i.e., GNPL-PDMAEMA, as a micro-/nanostructured support platform for surface bioactivity regulation (Fig. 5.3).

PDMAEMA and PMAA were synthesized by RAFT polymerization and functionalized with a thiol group via aminolysis reaction to form PDMAEMA-SH and PMAA-SH. With the free thiol group, PDMAEMA-SH was easily conjugated to GNPLs and PMAA was conjugated AuNPs. It was found that the maximum protein adsorption on the surface occurred at pH 7.0 and the amount of PPase is 359.9 ± 4.2 ng cm^{-2}. The adsorption decreased with increasing pH value. At pH 8.0 and 9.0, the adsorption values were about 65% and 33%, respectively. At pH 10.0, the GNPL-PDMAEMA surface could completely release the AuNP-PPase-PMAA conjugates and only less than 4% protein remained on the surfaces. The pH-dependent protein capture and release mechanism is mainly attributed to the interaction between the two pH responsive polymers: PDMAEMA and PMAA. The pKa of PDMAEMA is between 7.5 and 8.0 [30, 31]. Therefore, it is positively charged at pH 7.0 and negatively charged at pH 10.0. PMAA is negatively charged in the pH range of 6.0–10.0 due to fact that the PMAA carboxylic acid groups are in

the anionic form of –COO– [32]. We also showed that this "capture/release" effect is reversible by cyclic adjustment of the pH value between 7.0 and 10.0 for at least three times.

5.2 Regulation of Cell Behavior

It has been demonstrated that the surfaces on which cells reside and interact in vivo are rough and are composed of diverse three-dimensional micro-/nanostructures which are essential in maintaining cellular functions [33]. For example, extracellular matrix (ECM) and the inner surfaces of blood vessels are rough, with topographical features that affect protein adsorption and cellular responses [34, 35]. Lensen et al. found that poly(ethylene glycol) (PEG) hydrogel surfaces, which are intrinsically cell repellent, support the growth of L929 cells after introducing micro-/nanotopographical features in the surface [36]. Nanotopography has been shown to regulate the properties and behavior of human embryonic stem cells (hESCs), including cell morphology, adhesion, proliferation, and self-renewal [35]. Cardiovascular stents with micro-/nanotopographical surfaces were also found to endothelialize more effectively than those with smooth surfaces [37]. In addition, nanostructured surfaces modified with cell-specific ligands were significantly more efficient in the capture and isolation of circulating tumor cells [38, 39].

5.2.1 Maintaining the Pluripotency of ESCs on GNPLs with Nanoscale Surface Roughness

The influence of surface nanoscale features on the function of ESCs is attracting increasing attention because the features resemble those of the natural ECM where cells reside and interact [40]. Using photolithography Chen and coworkers prepared glass substrates with patterned surface roughness features of 70 and 150 nm and investigated the behavior of hESCs on these surfaces. They found that smooth glass was conducive to maintaining the self-renewal and pluripotency of hESCs in long-term culture; in contrast, the nanorough surfaces promoted spontaneous differentiation and loss of pluripotency [35]. In general, however, the influence of sub-microscale and microscale roughness on the maintenance of ESC pluripotency has not been much explored and remains unclear.

To address this question, we investigated the influence of surface roughness from nano- to submicro- to microscale on the maintenance of mouse ESC (mESC) pluripotency in long-term culture under feeder-free conditions [8]. GNPLs with nano-, sub-micro-, and microscale roughness were prepared by adjusting the volume of the gold plating solution (designated GL-1, GL-2, GL-3, GL-4, and GL-5 with increasing surface roughness). Undifferentiated ESCs can express the Oct-4 gene,

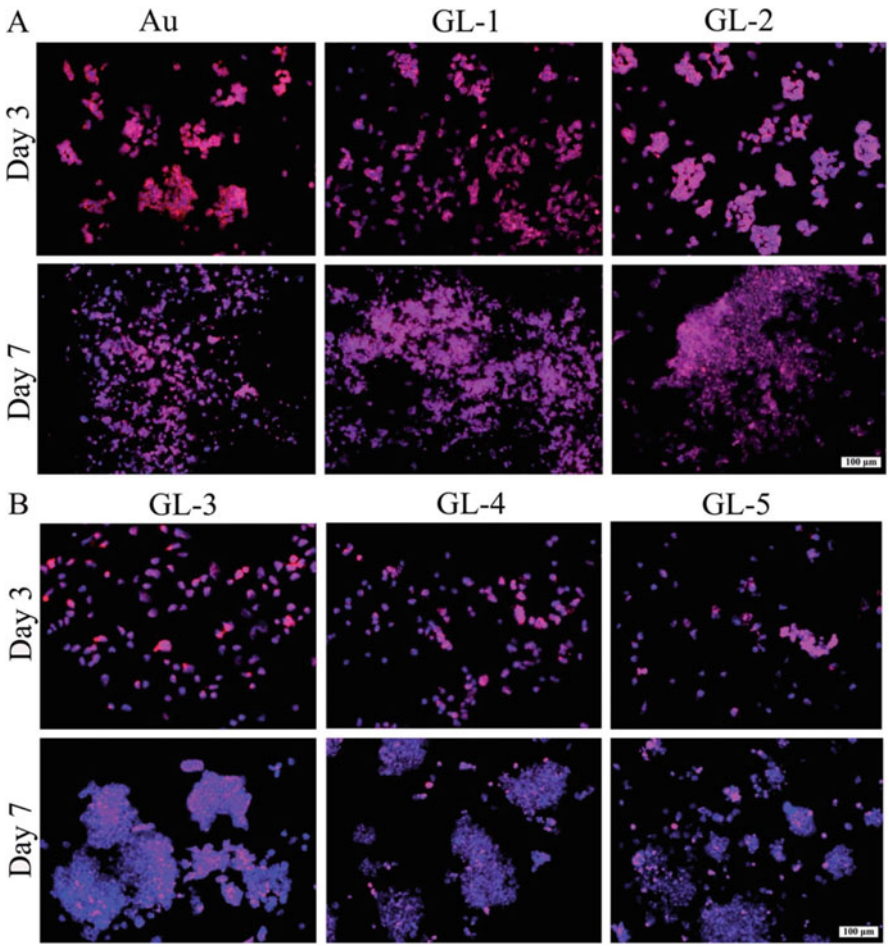

Fig. 5.4 Immunofluorescence images of mESCs cultured for 3 and 7 days on various surfaces. The cells were costained for Oct-4 (*red*) and nuclei (DAPI; *blue*). Undifferentiated mESCs were positively immunolabeled for Oct-4 and were stained *red*. DAPI (*blue* counterstain) labels all cells in the population; therefore, differentiated cell types appear *blue*. (**a**) *Au*, *GL-1*, and *GL-2*; (**b**) *GL-3*, *GL-4*, and *GL-5*. Bar, 100 μm. (Reprinted from Ref. [8] with permission. Copyright 2014 Royal Society of Chemistry)

which is essential for maintaining the cells in the undifferentiated state. Decreases in Oct-4 immunoreactivity signify cell differentiation. The majority of mESCs seeded on sAu, GL-1, and GL-2, whose surface roughness is less than 392 nm, retained their "stemness" after culture for 3 and 7 days, as shown by expression of the Oct-4 gene (Fig. 5.4a). In contrast, the pluripotency of cells cultured on GL-3, GL-4, and GL-5, with surface roughness greater than 573 nm, decreased from day 3; loss of pluripotency was greater after 7 days, particularly on microrough GL-5 (Fig. 5.4b). These results are consistent with data from quantitative polymerase

chain reaction (qPCR) analysis of Oct-4 expression: no significant loss of Oct-4 gene expression was observed in cells grown on nanorough GL-1 (~84%) compared with those on sAu. In contrast, Oct-4 gene expression decreased strongly on GL-3 (~73%) and GL-5 (~52%), with roughness greater than 573 nm. In sum these results show that sAu and GNPLs with low sub-microscale roughness (R_q less than 392 nm) supported very well the long-term pluripotency of mESC. However, GNPLs with sub-microscale surface roughness (R_q) greater than 573 nm and microscale surface roughness of 1205 nm decreased the pluripotency of the cells and accelerated their spontaneous differentiation, especially on microrough GNPL.

The signaling cascades engaged in topological sensing by mESCs were investigated by analyzing the expression of proteins related to E-cadherin-mediated cell–cell adhesion and the formation of integrin-mediated focal adhesions (FAs). It was found that mESCs cultured on sAu and nanorough GNPL (R_q, 106 nm) tended to form larger colonies with cells tightly connected with each other than cells on microrough GNPL. Also the cells maintained much stronger expression of E-cadherin than cells on microrough GNPL. In contrast, the ability of the cells cultured on microrough GNPL to form colonies was significantly decreased, and cells were distributed randomly with much weaker expression of E-cadherin (Fig. 5.5a, b). In addition, β-catenin was expressed exclusively in cells cultured on sAu and nanorough GNPLs, indicating the presence of strong adherens junctions that support E-cadherin-mediated cell–cell adhesions in mESC colonies. In comparison, the cells cultured on microrough GNPL showed much weaker expression of β-catenin (Fig. 5.5c). In focal adhesion (FA) analysis, mESCs exhibited much stronger expression of vinculin (a FA protein) on sAu and nanorough GNPL than on microrough GNPL. These results suggest that nanorough GNPL is conducive to the formation of FAs in mESCs, while microrough GNPL strongly inhibits FA formation, possibly resulting in faster spontaneous differentiation of the mESCs.

5.2.2 *Controlling Cell Behavior on GNPL Grafted with Protein-Resistant Polymers*

Despite much effort devoted to the investigation of the interactions between topography and cell behavior, cellular responses to topography are not well understood and results are contradictory in different experimental systems [41]. Many studies have shown that topographical surfaces increase cell adhesion and cell proliferation by affecting the distribution of ECM proteins adsorbed from the cell culture medium [42, 43] and by increasing protein adsorption [44]. Others believe that cellular responses do not rely only on the cell adhesion proteins or ligands in the local environment, that the topographical structure of the surface itself is important, and that protein adsorption alone does not determine cell behavior. For example, on a surface patterned with grooves overlaid with an orthogonal fibronectin pattern, osteoblasts were aligned predominantly with the grooves, regardless of the

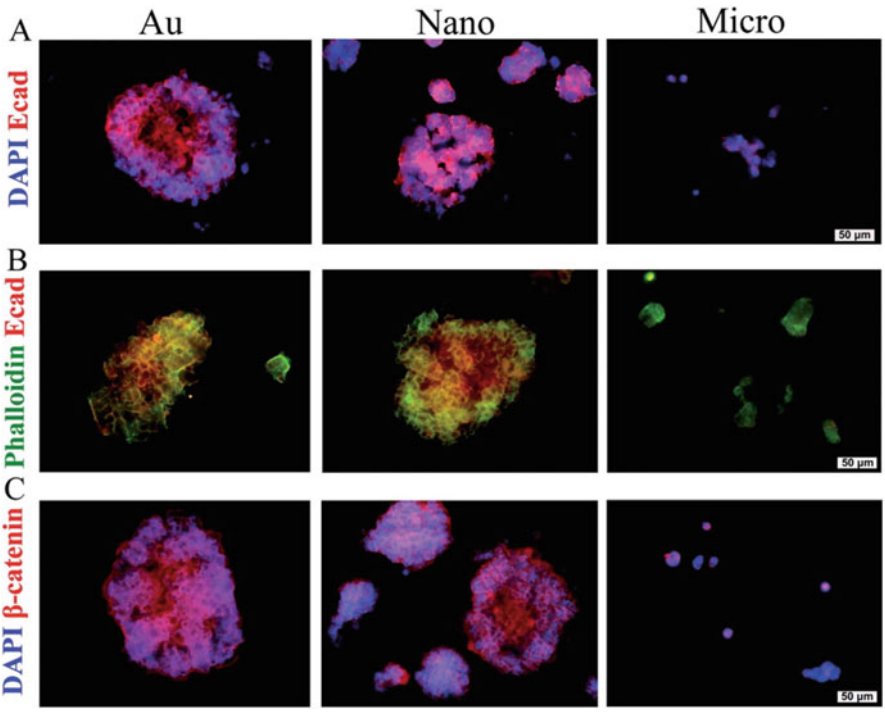

Fig. 5.5 Immunofluorescence images of mESCs on smooth Au and GNPLs with nanoscale and microscale surface roughness after culture for 3 days. (**a**) Cells costained for nuclei (*DAPI*, *blue*) and E-cadherin (*red*); (**b**) cells costained for cytoskeleton (phalloidin, *green*) and E-cadherin (*red*); (**c**) cells costained for nuclei (*DAPI*, *blue*) and *β-catenin* (*red*). Scale bar, 50 μm. (Reprinted from Ref. [8] with permission. Copyright 2014 Royal Society of Chemistry)

distribution of fibronectin (Fn), implying that the topography influenced the cell behavior independently of protein adsorption [45]. Dalby and coworkers showed that cell adhesion was quite different on 10 nm and 50 nm nanoscale islands on poly (*n*-butyl methacrylate)/poly(styrene) blend films [46].

To investigate the role of surface topology independent of other factors on cell behavior, we modified GNPL with POEGMA using SI-ATRP to obtain a topological surface having minimal protein adsorption [9]. Cell adhesion experiments were carried out using two cell types, human L02 hepatocytes and human hepatocellular carcinoma BEL-7402 cells. The cell density on GNPL was higher than on sAu, and after modification with POEGMA cell adhesion was reduced on both surfaces. However, whereas cell adhesion was greatly decreased on sAu, it was reduced by only ~50% for GNPL-POEGMA, and the density on GNPL-POEGMA was an order of magnitude higher than on sAu-POEGMA. L02 and BEL-7402 adhesion on sAu-POEGMA was lower by 92.8% and 97.7%, respectively, compared to sAu. For GNPL-POEGMA surface, the decrease in adhesion compared to GNPL was only 51.5% for L02 and 38.4% for BEL-7402 cells. These data showed that surface

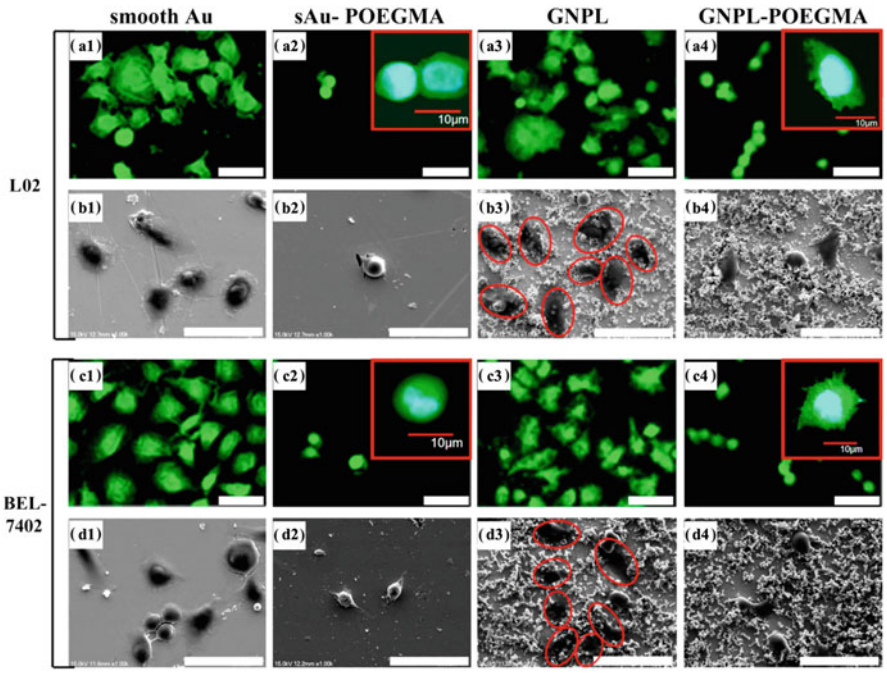

Fig. 5.6 Fluorescence images (**a1**-**a4**) and SEM images (**b1**-**b4**) of L02 cells and fluorescence images (**c1**-**c4**) and SEM images (**d1**-**d4**) of BEL-7402 cells on different surfaces. Spread cells on the GNPL surface are indicated by red ovals in **b3** and **d3**. The scale bar in all images is 50 μm. The shape and filopodia of the cells on POEGMA-modified surfaces were observed by confocal microscopy and are shown as insets in **a2**, **a4**, **c2**, and **c4**. Scale bar, 10 μm

topography is an important determinant of cell adhesion on protein-resistant POEGMA surfaces.

The combined effects of topography and protein resistance on cell–surface interactions were also investigated. Cell spreading was evaluated using fluorescent staining with Alexa Fluor 488 phalloidin (Fig. 5.6a, c). Spreading occurred on the sAu and GNPL surfaces. On the POEGMA-modified surfaces, cell spreading appeared to be constrained to some extent based on the spherical shape of the cells. However, spreading was quite different on the GNPL-POEGMA and sAu-POEGMA surfaces, as shown in the confocal microscopy images (Fig. 5.6 insets). Cells on GNPL-POEGMA showed small lamelipodia and short cell filopodia (Fig. 5.6a4, c4), whereas cells on sAu-POEGMA did not (Fig. 5.6a2, c2). Similar trends were found in SEM images (Fig. 5.6b, d). These results demonstrate that although cell spreading on protein-resistant surfaces was constrained, presumably because of the lack of adsorbed proteins, the cells on topographical surfaces were more firmly attached compared to those on smooth surfaces. In general, it was concluded that topography is more important than protein-resistant polymers for cell adhesion on a protein-resistant surface.

5.2.3 *Controlling Cell Behavior on GNPL Modified with Cell-Binding Ligands*

As well as surface topography, surface chemical modification has been shown to be effective in regulating cell behavior [47, 48]. To promote specific interactions between cells and material surfaces, cell-binding ligands such as arginine–glycine–aspartic acid (RGD) peptide have often been used [49, 50]. However, nonspecific adsorption of serum proteins can interfere with specific cell–ligand interactions. To avoid nonspecific adsorption of serum proteins, Causa and coworkers investigated cell-specific interactions with surfaces in serum-free medium [50]. However, serum contains many proteins and hormones that are vital for the maintenance of cell function. Therefore, studies under serum-free conditions cannot accurately reflect cell-specific interactions. To address this issue, we used protein-resistant polymer brushes (POEGMA) to modify GNPL via SI-ATRP and further modified the POEGMA with glycine–arginine–glycine–aspartic acid–tyrosine (GRGDY) peptide, a typical ligand that binds integrins and triggers specific cell responses [7]. It was found that the cell density on sAu was significantly higher than on GNPL (Fig. 5.7), suggesting that L929 fibroblasts prefer to adhere and proliferate on smooth surfaces. This observation is consistent with previously reported research [51]. We speculated that GNPL surface alters the native conformations of the adsorbed cell-adhesive proteins [52], thereby resulting in poor recognition and binding between the membrane integrins of L929 and those proteins. Hence, it is

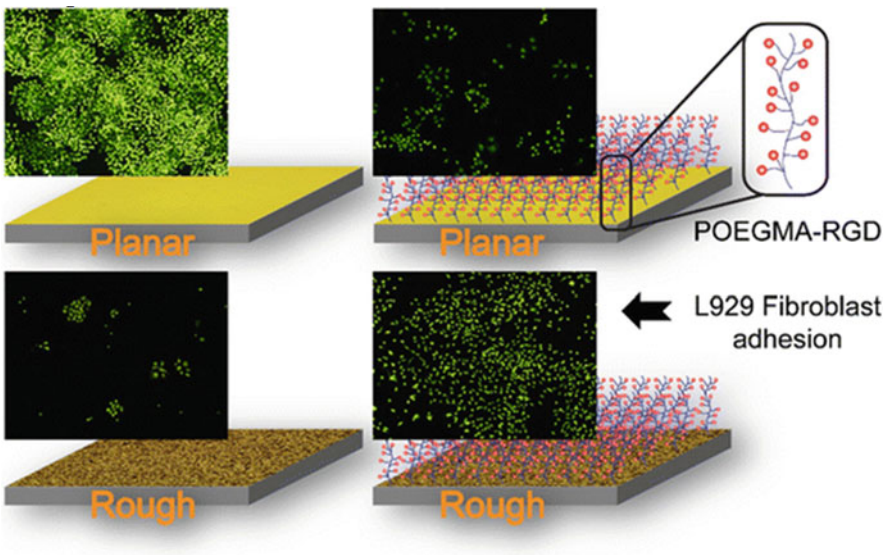

Fig. 5.7 Regulating the behavior of L929 fibroblasts on GNPL modified with POEGMA and cell-binding ligand GRGDY. (Reprinted from Ref. [7] with permission. Copyright 2012 Wiley-VCH)

difficult for L929 cells to form mature focal adhesions on GNPL surfaces, thereby further hindering cell adhesion, spreading, and proliferation.

The cell densities on all of the surfaces modified with POEGMA were significantly reduced and most adherent cells did not spread. A few cells aggregated to form small clusters, indicating that the surfaces were unfavorable for cell adhesion. However, after modification with GRGDY peptide, the cellular responses were totally reversed. The specific binding between cells and GRGDY greatly improved cell adhesion (Fig. 5.7). Cell densities on the GNPL-POEGMA-GRGDY surface were at least 131 ± 13 cells/mm^2 at 120 h. This value was much higher than on the unmodified and POEGMA-modified GNPLs and even higher than on sAu after the same treatment. Thus, it appeared that although the increased surface roughness was unfavorable for the adhesion of L929 cells, the much higher surface-to-volume ratio of the GNPL surface resulted in a higher density of surface immobilized molecules, and the enhanced specific interactions between cells and GRGDY peptides counteracted the negative effect of the roughness, resulting in improved cell adhesion and proliferation.

The cell density on GNPL with lower surface roughness (GNPL (a)) was higher than on the two GNPLs with higher surface roughness (GNPL (c) and GNPL (b); roughness: GNPL (c) > GNPL (b)), and it was the only GNPL that supported cell growth. It appears that surface roughness and cell-specific binding, having opposite effects, reached an optimal balance on GNPL (a). The densities of GRGDY peptide on GNPL (b) and (c) were higher than on GNPL (a) due to their higher surface-to-volume ratios. However, according to a study reported by Mann and West, a very high density of cell-binding ligands immobilized on surfaces is unfavorable for the proliferation of certain mesenchymal-derived cell types [53]. A similar phenomenon was observed by Bellis and coworkers [54, 55]. In our work [6], although the cell density on sAu-POEGMA-GRGDY surface also increased to 83 ± 8 cells/mm^2, it was still lower than on unmodified Au surface (310 ± 25 mm^2) (Fig. 5.7). This could be due to lower specific binding on the modified sAu surface compared to the modified GNPL surface; in addition, the POEGMA spacer reduced the adsorption of serum proteins including that of cell-adhesive proteins such as Fn.

5.2.4 *Capture of Circulating Cancer Cells Using Aptamer-Modified GNPL*

The measurement and analysis of circulating tumor cells (CTCs) can be regarded as a "liquid biopsy" of the tumor, providing insight into tumor biology in the critical window where intervention could actually make a difference [56]. However, CTCs are present in extremely low numbers in the bloodstream: typically one CTC cell per 10^5–10^7 normal blood cells [57]. Therefore, enrichment of CTCs is a prerequisite for CTC analysis. Over the past few decades, a diverse suite of technologies has been developed for isolating and counting CTCs in patient blood samples [58, 59]. The

known enhancement of cell–surface interactions, including cell adhesion, by micro-/nanostructuring can [60] be exploited for the enrichment and separation of CTCs. Aptamers (APTs), which may be considered as nucleic acid forms of traditional antibodies, can be designed to have specific affinity for given cell types. Moreover, APTs have been designed as efficient diagnostic probes for tumors both in vitro and in vivo [61]. Based on this knowledge, we modified GNPLs, first with POEGMA as an antifouling spacer using SI-ATRP; TD05 APT with high specific affinity for Ramos cells was then linked to the terminal hydroxyl groups of POEGMA by *N*, *N*′-disuccinimidyl carbonate (DSC) activation to give Au-POEGMA-APT and GNPL-POEGMA-APT surfaces. The B leukemia CTC cell, Ramos cell, was selected as a target to study the selective capture ability of cell-specific APT-modified GNPLs of varying surface roughness (designated GNPL1, GNPL2, and GNPL3 with increasing surface roughness) in cell mixtures containing Ramos and CEM cells (CL1014, T-cell line, human ALL) under serum-containing cell culture conditions [10].

The number of Ramos cells on the APT-modified GNPL surfaces increased with increasing surface roughness while the CEM cell number decreased, albeit slowly. The density of Ramos cells on the sAu, GNPL1, GNPL2, and GNPL3 surfaces were, respectively, 1.3-, 1.9-, 1.9-, and 2.2-fold greater than those of CEM cells. In contrast, after aptamer modification, the proportion of Ramos cells increased significantly with increasing surface roughness, with densities on the sAu, GNPL1, GNPL2, and GNPL3 surfaces, respectively, 2.2-, 2.8-, 3.0-, and 2.7-fold greater than those of CEM cells. We concluded that in serum-containing conditions, the roughness of the GNPLs enhanced the selectivity of the APT for Ramos cells. However, compared with serum-free conditions, the selectivity was still much weaker.

Serum is a highly complex fluid that contains many types of proteins which adsorb to surfaces nonspecifically and may “hide” the surface-immobilized APT to some extent, thereby further inhibiting the binding of cell receptors to the immobilized APT. This effect may be responsible, in large part, for the observed decrease in selectivity in serum compared to buffer. To improve the Ramos selectivity of the APT-modified surfaces in serum-containing conditions, we introduced POEGMA as a protein-resistant element. After POEGMA modification, the numbers of cells on Au-POEGMA and GNPL(1–3)-POEGMA were significantly reduced compared to the unmodified surfaces in serum-containing conditions. In addition, there was no observable difference in the numbers of Ramos and CEM cells. With the introduction of APT on the POEGMA, the density of Ramos cells increased significantly, whereas the density of CEM cells did not change. The density of Ramos cells on the four (sAu, GNPL1, GNPL2, and GNPL3) POEGMA surfaces modified with APT were, respectively, 0.9-, 1.5-, 3.5-, and 6.6-fold greater than those of CEM (Fig. 5.8).

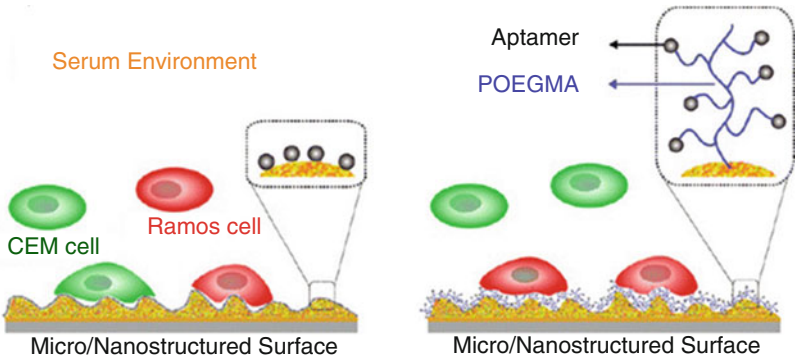

Fig. 5.8 Selective capture of Ramos cells in serum-containing conditions on GNPL surface modified with POEGMA and APT. (Reprinted from Ref. [10] with permission. Copyright 2013 American Chemical Society)

5.2.5 *Macromolecular Delivery to Cells Using GNPL via the Photoporation Effect*

Gold nanoparticle (GNP)-mediated photoporation has garnered increasing attention as a promising approach for macromolecular delivery to living cells [62–65]. When exposed to laser light of particular wavelengths, the membrane-associated GNPs convert the absorbed laser energy into heat, leading to increased membrane permeability and the transport of normally cell-impermeable macromolecules directly into the cytosol [66]. Additionally, by tuning the laser energy, the size of the pores created in the cell membrane by the GNPs can be varied, allowing control of the quantity and size of the molecules delivered [67]. Compared with traditional photoporation, in which cell membrane permeability is achieved by focusing high-intensity femtosecond (fs) laser pulses onto individual cells, GNP-mediated photoporation can be achieved at a lower laser energy with unfocused laser light that can irradiate a large number of cells, leading to greatly increased throughput [62]. Moreover, GNPs have superior chemical and biological properties including easy surface modification for molecular attachment and improved biocompatibility. Although effective, this method relies on complex and expensive equipment to generate laser light in short pulses [67]. Moreover, concerns remain because the extreme heating of the GNPs during irradiation may cause them to distort and fragment, resulting in high cytotoxicity [68, 69]. To solve these problems, we developed a new platform for macromolecular delivery that retains the photothermal properties of GNPs while avoiding the side effects caused by their entry into the cells. Instead of free GNPs, we used GNPLs as the photoporation "reagent." GNPLs, composed of numerous GNPs with nano- and microtopography, provide multiple sites for contact between cell membranes and the GNPs. We therefore hypothesized that GNPLs may serve as a novel and versatile macromolecular delivery platform upon irradiation with continuous-wave (CW) laser light (Fig. 5.9) [70].

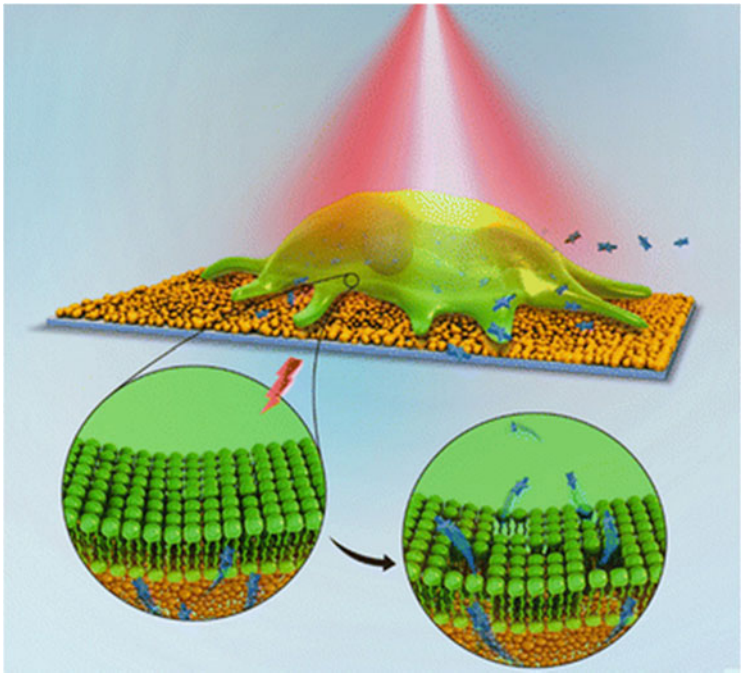

Fig. 5.9 A novel platform for macromolecular delivery into cells using gold nanoparticle layers via the photoporation effect. (Reprinted from Ref. [70], copyright 2016, WILEY-VCH Verlag GmbH & Co)

We first tried delivery of dextran to cells using this approach. Tetramethylrhodamine isothiocyanate (TRITC)-labeled dextran (red fluorescence), with a molecular weight of 4.4 kDa, was used as a model macromolecule and HeLa cells as model cells. It was found that without laser irradiation, dextran did not enter the cells efficiently; no red fluorescence was observed. Strong red fluorescence began to be observed at 3.2 W cm^{-2}/45 s, and the fluorescence intensity increased further at 5.1 W cm^{-2}/30 s. Decrease in irradiation time to 20 s at 5.1 W cm^{-2} failed to give high fluorescence intensity. The delivery efficiency in presence of sAu under those conditions was much lower. To further demonstrate the efficient delivery of TRITC-dextran to HeLa cells, we obtained confocal microscopy images using the Z-stack mode to view the distribution of TRITC-dextran. Scans were taken from top to bottom of the cell membrane. The images indicated that macromolecules entered the interior of the cells and were not merely attached to the cell membrane. Moreover, cell viability experiments demonstrated that vitality was maintained under these conditions.

Plasmid DNA (pDNA) is a commonly used gene carrier and its efficient delivery to living cells is essential for gene therapy. However, due to its large size and the necessity for transport into the nucleus, transfection is more difficult with pDNA than with dextran or RNA. In our work, the applicability of GNPL-laser irradiation

for the delivery of pDNA encoding green fluorescent protein (GFP), a widely used pDNA model that can easily transfect HeLa cells, was assessed. Lipofectamine 2000 (Lipo2000) complexed with pDNA was used as a standard cell transfection agent (positive control) because Lipo2000 is a widely used, commercially available transfection reagent for delivery of pDNA and RNA into cells [71]. It was found that under irradiation conditions 3.2 W cm^{-2}/45 s and 5.1 W cm^{-2}/30 s, virtually 100% of the HeLa cells gave a green fluorescence signal, suggesting the successful delivery and expression of pDNA in the cells. These results are in line with data from flow cytometry. Compared with 3.2 W cm^{-2}/45 s, the transfection efficiency at 5.1 W cm^{-2}/30 s was significantly higher; the cells showed stronger green fluorescence, similar to that obtained using Lipo2000. These results show that under laser irradiation, our platform based on GNPLs achieved direct and efficient delivery of pDNA to HeLa cells without compromising cell viability. Moreover, the transfection efficiency of this vector-free system was comparable to that of Lipo2000.

Gene delivery to different cell types has resulted in advances in the understanding of gene function and the development of genetic therapies [72–74]. Although Lipo2000 is effective for the transfection of many cell types, it is ineffective for the transfection of hard-to-transfect cell types such as primary cells including mouse embryonic fibroblasts (mEFs) used widely in stem cell research and human umbilical vein endothelial cells (HUVECs), which are used for endothelial cell physiology and pathology studies. Therefore, we investigated the delivery of pDNA to hard-to-transfect mEFs and HUVECs. Efficient intracellular delivery to mEFs has previously been challenging. For example, the transfection efficiencies of mEFs with pDNA using pDNA/magnetic nanoparticles and optimized electroporation were reported as ~11% [75] and ~40% [76], respectively. It was shown that pDNA was delivered to and expressed in mEFs under irradiation conditions of 3.2 W cm^{-2}/45 s with a transfection efficiency of approximately 39%, much higher than the ~19% using Lipo2000 ($p < 0.001$). At 5.1 W cm^{-2}/30 s, the transfection efficiency was further enhanced to 53% ($p < 0.001$, vs Lipo2000), and the fluorescence intensity was much higher than for Lipo2000 ($p < 0.001$). In addition, cell viability both immediately after and 24 h after laser irradiation was higher than 95% under both conditions. For HUVECs, sufficient intracellular delivery of pDNA could not be achieved using GNPL along probably because of the differences in cell type and size. The average size of HUVECs is only about 35% of the average size of mEFs meaning there are more sites for the contact between mEFs and GNPL surfaces than that between HUVECs and GNPL surfaces. To address this problem, we combined Lipo2000 and GNPL where pDNA was complexed with Lipo2000 before exposure to laser irradiation. At 5.1 W cm^{-2}/30 s, we achieved a transfection efficiency of ~44%, much higher than ~8% from using Lipo2000 alone ($p < 0.001$). Altogether, these data demonstrate that this system is effective for the pDNA transfection of hard-to-transfect cell types with an efficiency much higher than for Lipo2000 alone.

5.2.6 *Macromolecular Delivery to "Recalcitrant" Cells Using PEI and GNPL via the Photoporation Effect*

Using GNPL-assisted photoporation, we have achieved relatively high delivery efficiency of pDNA to hard-to-transfect mEFs (~53%) and HUVECs (~44%). However, there is still room to further improve the delivery efficiently. Polyethylenimine (PEI) is a representative synthetic nonviral gene carrier with superior transfection efficiency due to its unique "proton sponge effect" for endosomal escape of the gene payload [77]. The commercially available 25 kDa branched PEI (bPEI) in particular has been widely considered as the "gold standard" carrier for gene delivery [78]. Unfortunately, such high molecular weight (MW) PEI (HPEI) is generally cytotoxic, thus limiting its application. Low MW PEI (LPEI, MW <2 kDa) is acceptable with respect to cytotoxicity but has low transfection efficiency. Considerable efforts have been made to prepare novel PEI derivatives to overcome these limitations [79–81]. However, safe and efficient delivery systems for hard-to-transfect primary cell lines have rarely been reported. After confirming the potential of GNPL to serve as a universal macromolecular delivery platform [70], here we explored the possibility of combing LPEI with GNPL for safe and high-efficient pDNA delivery specifically to hard-to-transfect primary cell lines (mEFs and HUVECs) (Fig. 5.10). In this platform, LPEI serves as a carrier of pDNA to protect it from degradation. Laser-activated GNPL serves as a membrane disruption agent [82].

We achieved a very high pDNA transfection efficiency of 94.0 ± 6.3% to HUVECs when we added LPEI/pDNA complexes with a N/P of 20 to cells growing on GNPL under laser irradiation. Cell viability under this condition was very well

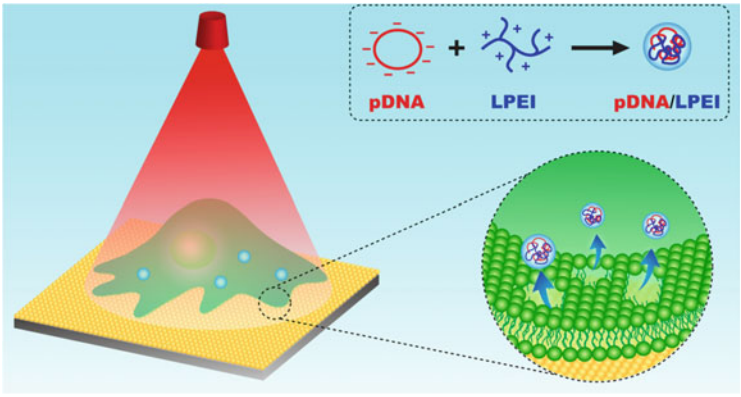

Fig. 5.10 LPEI/pDNA complex is formed by electrostatic interactions. Targeted cells are cultured on the GNPL, and then exposed to laser irradiation to enhance the permeability of the cell membrane, thereby assisting the diffusion of LPEI/pDNA complex from the surrounding medium into the cell. (Reprinted from Ref. [82] with permission. Copyright 2017 American Chemical Society)

maintained at ~100%, 48 h after transfection. The transfection value is higher than the value achieved using 25k PEI (75.1 ± 18.6%). Moreover, cell viability 48 h after transfection using 25k bPEI decreased to less than 5%, much lower than the viability of our system ($p < 0.001$). These results showed that LPEI/GNPL collaborative delivery system significantly outperformed the golden standard-25k bPEI for the delivery of pDNA to HUVECs. It is worth noting that this efficiency is also much higher than the efficiency achieved by complexing pDNA with Lipo2000 before exposure to GNPL-assisted laser irradiation (~44%).

We further investigated the delivery of pDNA to mEFs. Similar to HUVECs, our system gave high transfection efficiency (88.5 ± 9.2%) and high cell viability (99.8 ± 4.1%, 48 h after transfection) for mEFs. Last, we used our platform to deliver functional pDNA to illustrate its potential for endothelialization of artificial blood [83]. For this purpose, ZNF580 gene, which codes for a zinc finger protein, was chosen. This protein plays a critical role in alleviating atherosclerosis and has been shown to promote the proliferation and migration of endothelial cells [84]. Our data indicated that 48 h after transfection, the relative ZNF580 microRNA (mRNA) content was ~1.3 times higher than that of the negative control group. Moreover, transfection with pZNF580 resulted in an increase in initial attachment and a significant increase in long-term proliferation of HUVECs. In particular, after 48 h culture, the density of adherent pZNF580 transfected cells was about twice that of nontransfected cells ($p < 0.05$). These data suggest that our transfection method can effectively deliver pZNF580 to HUVECs such that proliferation for revascularization purposes may be enhanced. Together, we showed that our LPEI/GNPL collaborative delivery system provides a highly efficient and relatively simple approach for intracellular delivery, especially for hard-to-transfect cell lines that are difficult to treat using more traditional methods.

5.2.7 *GNPL-Based Regenerable Smart Antibacterial Surfaces*

Attachment and subsequent colonization by bacteria on the surfaces of synthetic materials and devices pose serious problems in both human healthcare and industrial applications [85, 86]. Antibacterial surfaces with capability to prevent bacterial attachment and biofilm formation have been a longstanding focus of research [87–91]. However, conventional antibacterial surfaces are becoming less effective due to the emergence of multidrug resistant bacteria [92]. Photothermal therapy using strong light absorbers to generate local heat for physical destruction of bacteria provides a promising approach for circumventing the problem of antibiotic resistance [93–98]. However, these photothermal antibacterial coatings suffer from the same inherent drawbacks as traditional antibacterial surfaces based on contact-killing mechanisms, and even if they show high bactericidal efficiency, they remain contaminated by dead bacteria and other debris, which not only provide nutrients for

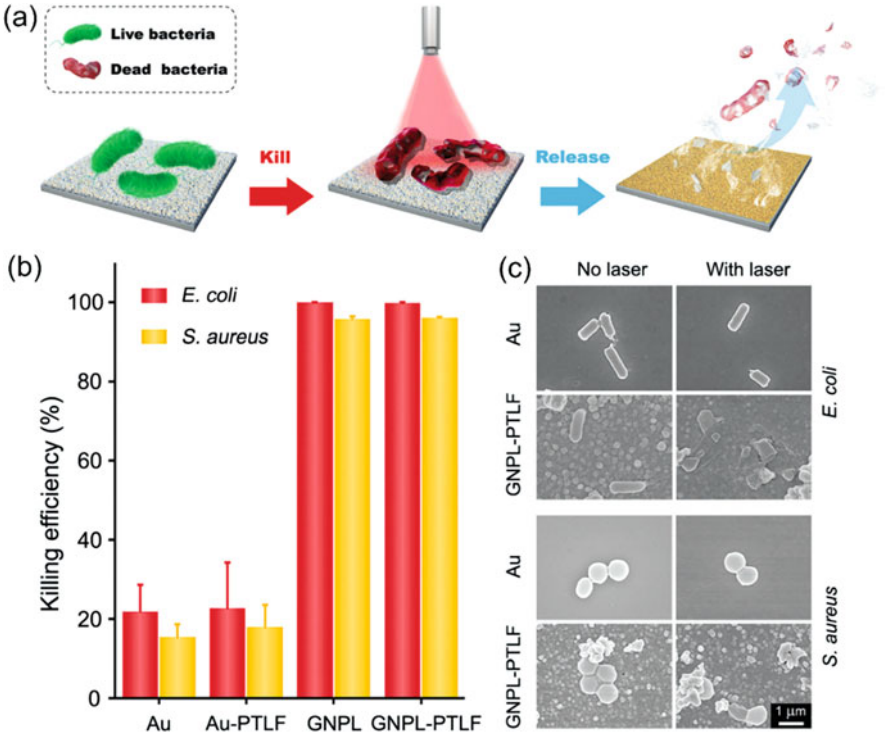

Fig. 5.11 (**a**) Schematic illustration of a smart antibacterial surface based on a GNPL-PTLF hybrid film with photothermal bacteria-killing capability and Vc-triggered bacteria-releasing ability. (**b**) Photothermal bactericidal activity of surfaces against *E. coli* and *S. aureus* under NIR laser irradiation (2.3 W/cm^2, 5 min) evaluated using a colony counting assay. Error bars represent the standard deviation of the mean ($n = 3$). (**c**) Typical SEM images of attached bacteria on Au and GNPL-PTLF surfaces with/without NIR laser irradiation. (Reprinted from Ref. [103] with permission. Copyright 2018 Royal Society of Chemistry)

subsequent bacterial interactions, but may also trigger severe immune responses and inflammation [99]. To circumvent the problem of dead bacteria, a promising "kill-and-release" strategy has been proposed for the development of smart antibacterial surfaces with the capability of not only killing the attached bacteria but also releasing dead bacteria and debris "on demand" under an appropriate stimulus [100–102]. To the best of our knowledge, smart photothermal antibacterial surfaces have not been developed yet. To fill this gap, we developed the first smart photothermal antibacterial surfaces with bacteria-releasing properties [103].

This smart coating is composed of two functional layers (Fig. 5.11a). The first is a gold nanoparticle layer (GNPL) composed of GNP aggregates which serve as the photothermal bactericidal agent. Compared with dispersed GNPs, the aggregated GNPs exhibit a more efficient photothermal effect due to the redshifted absorption [104]. In addition, the GNPL possesses a unique micro-nanotopography that provides multiple sites for contact with bacteria and facilitates local hyperthermia

induced by NIR laser irradiation. We anticipate that the GNPL can also be used as an effective antibacterial material on which attached bacteria can be destroyed photothermally. In addition, the GNPL was coated with a thin phasetransitioned lysozyme film (PTLF) as a contamination releasing layer. PTLF was recently developed in our previous works as a novel biocompatible two-dimensional (2D) proteinaceous nanofilm with versatile applications. For substrates immersed in phase-transitioned lysozyme solution, a PTLF composed of densely aggregated oligomers within amyloid-like structures was shown to form on the surface in a few minutes. Such PTLFs are transparent and exhibit strong substrate bonding even in extreme pH conditions or under gas plasma treatment [105, 106].

It is thus expected that the addition of PTLF will not affect the light-to-heat conversion capability of the GNPL or the bactericidal efficacy of the GNPL. Our results showed that more than 99% of attached Gram-positive *S. aureus* or Gram-negative *E. coli* were killed under near infrared laser radiation at 2.3 W/cm^2 for 5 min (Fig. 5.11b, c). we also showed that the degradation of PTLF can be triggered in a closely controlled manner by treatment with vitamin C (Vc). Almost all of the killed bacteria could be removed by incubating the surface in Vc solution for a short time period of 10 min due to the degradation of the topmost layer of PTLF. Moreover, the GNPL-PTLF coating can be used repeatedly over at least three "kill-and-release" cycles, which is of particular importance for long-term usage.

5.3 Summary and Outlook

Gold nanoparticle layers, as a representative material with surface topological structures, have a direct influence on protein adsorption/activity and cell behavior including adhesion, spreading, proliferation, and differentiation. Compared to smooth gold surfaces, GNPLs, due to their "three-dimensional" structure, offer better access for the binding of biomacromolecules such as proteins, antigens, and antibodies and favor the maintenance of their conformation and bioactivity, thereby improving cell adhesion further. In combination with protein-resistant polymers and specific ligands for certain types of proteins or cells, modified GNPL can selectively bind certain proteins and cells from protein and cell mixtures, including the highly complex environment of serum. In combination with stimuli-responsive polymers such as pH-sensitive polymers, modified GNPL can achieve multifunction such as recyclable protein capture and release. In addition, under laser irradiation, GNPLs show excellent photothermal property. This feature endows GNPLs with the ability to serve as a novel and efficient platform for the delivery of various macromolecules to different cell types including hard-to-transfect cell types. It also provides GNPLs with the opportunity to serve as an efficient and antibiotic-free antibacterial coating with the potential to kill and remove adherent bacteria, particularly multidrug resistant bacteria, on the surfaces of medical devices. It is concluded that GNPLs hold great promise in many biomedical fields such as protein detection, regulation of

protein and cell behavior, capture of circulating cancer cells, macromolecular delivery to living cells, and antibacterial applications.

Acknowledgments This work was supported by the National Natural Science Foundation of China (21774086, 22175125, and 21935008) and the Natural Science Foundation of the Jiangsu Higher Education Institutions of China (21KJA150008). We thank Prof. John Brash for the helpful discussion.

References

1. Yuan L, Yu Q, Li D. Chen H surface modification to control protein/surface interactions. Macromol Biosci. 2011;11:1031–40.
2. Gittens RA, McLachlan T, Olivares-Navarrete R, Cai Y, Berner S, Tannenbaum R, Schwartz Z, Sandhage KH. Boyan B D the effects of combined micron-/submicron-scale surface roughness and nanoscale features on cell proliferation and differentiation. Biomaterials. 2011;32:3395–403.
3. Chen W, Weng S, Zhang F, Allen S, Li X, Bao L, Lam RH, Macoska JA, Merajver SD. Fu J Nanoroughened surfaces for efficient capture of circulating tumor cells without using capture antibodies. ACS Nano. 2013;7:566–75.
4. Yu Q, Ista LK, Gu R, Zauscher S, Lopez GP. Nanopatterned polymer brushes: conformation, fabrication and applications. Nanoscale. 2016;8:680–700.
5. Zhou F, Yuan L, Wang H, Li D, Chen H. Gold nanoparticle layer: a promising platform for ultra-sensitive cancer detection. Langmuir. 2011;27:2155–8.
6. Zhou F, Wang M, Yuan L, Cheng Z, Wu Z, Chen H. Sensitive sandwich ELISA based on a gold nanoparticle layer for cancer detection. Analyst. 2012;137:1779–84.
7. Zhou F, Li D, Wu Z, Song B, Yuan L, Chen H. Enhancing specific binding of L929 fibroblasts: effects of multi-scale topography of GRGDY peptide modified surfaces. Macromol Biosci. 2012;12:1391–400.
8. Lyu Z, Wang H, Wang Y, Ding K, Liu H, Yuan L, Shi X, Wang M, Wang Y, Chen H. Maintaining the pluripotency of mouse embryonic stem cells on gold nanoparticle layers with nanoscale but not microscale surface roughness. Nanoscale. 2014;6:6959–69.
9. Shi X, Wang Y, Li D, Yuan L, Zhou F, Wang Y, Song B, Wu Z, Chen H, Brash JL. Cell adhesion on a POEGMA-modified topographical surface. Langmuir. 2012;28:17011–8.
10. Wang Y, Zhou F, Liu X, Yuan L, Li D, Wang Y, Chen H. Aptamer-modified micro/nanostructured surfaces: efficient capture of Ramos cells in serum environment. ACS Appl Mater Interfaces. 2013;5:3816–23.
11. Wu J, Qu Y, Yu Q, Chen H. Gold nanoparticle layer: a versatile nanostructured platform for biomedical applications. Mater Chem Front. 2018;2:2175–90.
12. Zhang Q, Xu JJ, Liu Y, Chen HY. In-situ synthesis of poly(dimethylsiloxane)-gold nanoparticles composite films and its application in microfluidic systems. Lab Chip. 2008;8:352–7.
13. Bai HJ, Shao ML, Gou HL, Xu JJ, Chen HY. Patterned au/poly(dimethylsiloxane) substrate fabricated by chemical plating coupled with electrochemical etching for cell patterning. Langmuir. 2009;25:10402–7.
14. Wang B, Chen K, Jiang S, Reincke F, Tong W, Wang D, Gao C. Chitosan-mediated synthesis of gold nanoparticles on patterned poly(dimethylsiloxane) surfaces. Biomacromolecules. 2006;7:1203–9.
15. Drummond TG, Hill MG, Barton JK. Electrochemical DNA sensors. Nat Biotechnol. 2003;21:1192–9.

16. Nam JM, Thaxton CS, Mirkin CA. Nanoparticle-based bio-bar codes for the ultrasensitive detection of proteins. Science. 2003;301:1884–6.
17. Webster TJ, Schadler LS, Siegel RW, Bizios R. Mechanisms of enhanced osteoblast adhesion on nanophase alumina involve vitronectin. Tissue Eng. 2001;7:291–301.
18. Brigger I, Dubernet C, Couvreur P. Nanoparticles in cancer therapy and diagnosis. Adv Drug Deliv Rev. 2012;64:24–36.
19. Roach P, Farrar D, Perry CC. Surface tailoring for controlled protein adsorption: effect of topography at the nanometer scale and chemistry. J Am Chem Soc. 2006;128:3939–45.
20. Eteshola E, Leckband D. Development and characterization of an ELISA assay in PDMS microfluidic channels. Sens Actuators, B. 2017;18:129–33.
21. Jia CP, Zhong XQ, Hua B, Liu MY, Jing FX, Lou XH, Yao SH, Xiang JQ, Jin QH, Zhao JL. Nano-ELISA for highly sensitive protein detection. Biosens Bioelectron. 2009;24:2836–41.
22. Park JS, Cho MK, Lee EJ, Ahn KY, Lee KE, Jung JH, Cho Y, Han SS, Kim YK, Lee JA. Highly sensitive and selective diagnostic assay based on virus nanoparticles. Nat Nanotechnol. 2009;4:259–64.
23. Dixit CK, Vashist SK, O'Neill FT, O'Reilly B, BD MC, O'Kennedy R. Development of a high sensitivity rapid Sandwich ELISA procedure and its comparison with the conventional approach. Anal Chem. 2010;48:7049–52.
24. Jonkheijm P, Weinrich D, Schroder H, Niemeyer CM, Waldmann H. Chemical strategies for generating protein biochips. Angew Chem Int Ed. 2008;47:9618–47.
25. Xu FJ, Neoh KG, Kang ET. Bioactive surfaces and biomaterials via atom transfer radical polymerization. Prog Polym Sci. 2009;34:719–61.
26. Sproule TL, Alex Lee J, Li H, Lannutti JJ, Tomasko DL. Bioactive polymer surfaces via supercritical fluids. J Supercrit Fluids. 2004;28:241–8.
27. Li Z, Liu F, Yuan Y, Wu J, Wang H, Yuan L, Chen H. Multifunctional gold nanoparticle layers for controllable capture and release of proteins. Nanoscale. 2017;9:15407–15.
28. Sundaram HS, Ella-Menye J-R, Brault ND, Shao Q, Jiang S. Reversibly switchable polymer with cationic/zwitterionic/anionic behavior through synergistic protonation and deprotonation. Chem Sci. 2014;5:200–5.
29. Kumar S, Tong X, Dory YL, Lepage M, Zhao YA. CO_2-switchable polymer brush for reversible capture and release of proteins. Chem Commun. 2013;49:90–2.
30. Qiu X, Hu S. "Smart" materials based on cellulose: a review of the preparations, properties, and applications. Materials. 2013;6:738–81.
31. Qiao Y, Huang Y, Qiu C, Yue X, Deng L, Wan Y, Xing J, Zhang C, Yuan S, Dong A, Xu J. The use of PEGylated poly[2-(*N*,*N*-dimethylamino)ethyl methacrylate] as a mucosal DNA delivery vector and the activation of innate immunity and improvement of HIV-1-specific immune responses. Biomaterials. 2010;31:115–23.
32. Lu W, Ma W, Lu J, Li X, Zhao Y, Chen G. Microwave-assisted synthesis of glycopolymer-functionalized silver nanoclusters: combining the bioactivity of sugar with the fluorescence and cytotoxicity of silver. Macromol Rapid Commun. 2014;35:827–33.
33. Ross AM, Jiang Z, Bastmeyer M, Lahann J. Physical aspects of cell culture substrates: topography, roughness, and elasticity. Small. 2012;8:336–55.
34. Dolatshahi-Pirouz A, Jensen T, Kraft DC, Foss M, Kingshott P, Hansen JL, Larsen AN, Chevallier J, Besenbacher F. Fibronectin adsorption, cell adhesion, and proliferation on nanostructured tantalum surfaces. ACS Nano. 2010;4:2874–82.
35. Chen W, Villa-Diaz LG, Sun Y, Weng S, Kim JK, Lam RH, Han L, Fan R, Krebsbach PH, Fu J. Nanotopography influences adhesion, spreading, and self-renewal of human embryonic stem cells. ACS Nano. 2012;6:4094–103.
36. Schulte V, Dıéz M, Möller M, Lensen M. Surface topography induces fibroblast adhesion on intrinsically nonadhesive poly(ethylene glycol) substrates. Biomacromolecules. 2009;10:2795–801.

37. Loya MC, Brammer KS, Choi C, Chen LH, Jin S. Plasma-induced nanopillars on bare metal coronary stent surface for enhanced endothelialization. Acta Biomater. 2010;6:4589–95.
38. Chen L, Liu X, Su B, Li J, Jiang L, Han D, Wang S. Aptamer-mediated efficient capture and release of T lymphocytes on nanostructured surfaces. Adv Mater. 2011;23:4376–80.
39. Sekine J, Luo SC, Wang S, Zhu B, Tseng HR, Yu HH. Functionalized conducting polymer nanodots for enhanced cell capturing: the synergistic effect of capture agents and nanostructures. Adv Mater. 2011;23:4788–92.
40. Lee MR, Kwon KW, Jung H, Kim HN, Suh KY, Kim K, Kim KS. Direct differentiation of human embryonic stem cells into selective neurons on nanoscale ridge/groove pattern arrays. Biomaterials. 2010;31:4360–6.
41. Cretel E, Pierres A, Benoliel AM, Bongrand P. How cells feel their environment: a focus on early dynamic events. Cell Mol Bioeng. 2008;1:5–14.
42. Chen H, Song W, Zhou F, Wu Z, Huang H, Zhang J, Lin Q, Yang B. The effect of surface microtopography of poly(dimethylsiloxane) on protein adsorption, platelet and cell adhesion. Colloids Surf B Biointerfaces. 2009;71:275–81.
43. Yamamoto S, Tanaka M, Sunami H, Arai K, Takayama A, Yamashita S, Morita Y, Shimomura M. Relationship between adsorbed fibronectin and cell adhesion on a honeycomb-patterned film. Surf Sci. 2006;600:3785–91.
44. Rechendorff K, Hovgaard MB, Foss M, Zhdanov VP, Besenbacher F. Enhancement of protein adsorption induced by surface roughness. Langmuir. 2006;22:10885–8.
45. Charest JL, Eliason MT, Garcia AJ, King WP. Combined microscale mechanical topography and chemical patterns on polymer cell culture substrates. Biomaterials. 2006;27:2487–94.
46. Dalby MJ, Riehle MO, Johnstone HJ, Affrossman S, Curtis AS. Nonadhesive nanotopography: fibroblast response to poly(*n*-butyl methacrylate)-poly(styrene) demixed surface features. J Biomed Mater Res A. 2003;67:1025–32.
47. Marcon L, Spriet C, Coffinier Y, Galopin E, Rosnoblet C, Szunerits S, Heliot L, Angrand PO, Boukherroub R. Cell adhesion properties on chemically micropatterned boron-doped diamond surfaces. Langmuir. 2010;26:15065–9.
48. Lagunas A, Comelles J, Martinez E, Samitier J. Universal chemical gradient platforms using poly(methyl methacrylate) based on the biotin-streptavidin interaction for biological applications. Langmuir. 2010;26:14154–61.
49. Li B, Chen J, Wang JH. RGD peptide-conjugated poly(dimethylsiloxane) promotes adhesion, proliferation, and collagen secretion of human fibroblasts. J Biomed Mater Res A. 2006;79:989–98.
50. Causa F, Battista E, Della Moglie R, Guarnieri D, Iannone M, Netti PA. Surface investigation on biomimetic materials to control cell adhesion: the case of RGD conjugation on PCL. Langmuir. 2010;26:9875–84.
51. Kunzler TP, Drobek T, Schuler M, Spencer ND. Systematic study of osteoblast and fibroblast response to roughness by means of surface-morphology gradients. Biomaterials. 2007;28:2175–82.
52. Lord MS, Cousins BG, Doherty PJ, Whitelock JM, Simmons A, Williams RL, Milthorpe BK. The effect of silica nanoparticulate coatings on serum protein adsorption and cellular response. Biomaterials. 2006;27:4856–62.
53. Mann BK, West JL. Cell adhesion peptides alter smooth muscle cell adhesion, proliferation, migration, and matrix protein synthesis on modified surfaces and in polymer scaffolds. J Biomed Mater Res. 2002;60:86–93.
54. Sawyer AA, Weeks DM, Kelpke SS, McCracken MS, Bellis SL. The effect of the addition of a polyglutamate motif to RGD on peptide tethering to hydroxyapatite and the promotion of mesenchymal stem cell adhesion. Biomaterials. 2005;26:7046–56.
55. Sawyer AA, Hennessy KM, Bellis SL. The effect of adsorbed serum proteins, RGD and proteoglycan-binding peptides on the adhesion of mesenchymal stem cells to hydroxyapatite. Biomaterials. 2007;28:383–92.

56. Wang S, Liu K, Liu J, Yu ZT, Xu X, Zhao L, Lee T, Lee EK, Reiss J, Lee YK, Chung LW, Huang J, Rettig M, Seligson D, Duraiswamy KN, Shen CK, Tseng HR. Highly efficient capture of circulating tumor cells by using nanostructured silicon substrates with integrated chaotic micromixers. Angew Chem Int Ed. 2011;50:3084–8.
57. Alunni-Fabbroni M, Sandri MT. Circulating tumour cells in clinical practice: methods of detection and possible characterization. Methods. 2010;50:289–97.
58. Nagrath S, Sequist LV, Maheswaran S, Bell DW, Irimia D, Ulkus L, Smith MR, Kwak EL, Digumarthy S, Muzikansky A, Ryan P, Balis UJ, Tompkins RG, Haber DA, Toner M. Isolation of rare circulating tumour cells in cancer patients by microchip technology. Nature. 2007;450:1235–9.
59. Adams AA, Okagbare PI, Feng J, Hupert ML, Patterson D, Gottert J, McCarley RL, Nikitopoulos D, Murphy MC, Soper SA. Highly efficient circulating tumor cell isolation from whole blood and label-free enumeration using polymer-based microfluidics with an integrated conductivity sensor. J Am Chem Soc. 2008;130:8633–41.
60. Fischer KE, Aleman BJ, Tao SL, Hugh Daniels R, Li EM, Bunger MD, Nagaraj G, Singh P, Zettl A, Desai TA. Biomimetic nanowire coatings for next generation adhesive drug delivery systems. Nano Lett. 2009;9:716–20.
61. Medley CD, Bamrungsap S, Tan W, Smith JE. Aptamer-conjugated nanoparticles for cancer cell detection. Anal Chem. 2011;83:727–34.
62. Qin Z, Bischof JC. Thermophysical and biological responses of gold nanoparticle laser heating. Chem Soc Rev. 2012;41:1191–217.
63. Sapsford KE, Algar WR, Berti L, Gemmill KB, Casey BJ, Oh E, Stewart MH, Medintz IL. Functionalizing nanoparticles with biological molecules: developing chemistries that facilitate nanotechnology. Chem Rev. 2013;113:1904–2074.
64. Qu Y, Zhang Y, Yu Q, Chen H. Surface-mediated intracellular delivery by physical membrane disruption. ACS Appl Mater Interfaces. 2020;12:31054–78.
65. Qu Y, Lu K, Zheng Y, Huang C, Wang G, Zhang Y, Yu Q. Photothermal scaffolds/surfaces for regulation of cell behaviors. Bioact Mater. 2022;8:449–77.
66. Delcea M, Sternberg N, Yashchenok AM, Georgieva R, Baumler H, Mohwald H, Skirtach AG. Nanoplasmonics for dual-molecule release through nanopores in the membrane of red blood cells. ACS Nano. 2012;6:4169–80.
67. Xiong R, Raemdonck K, Peynshaert K, Lentacker I, De Cock I, Demeester J, De Smedt SC, Skirtach AG, Braeckmans K. Comparison of gold nanoparticle mediated photoporation: vapor nanobubbles outperform direct heating for delivering macromolecules in live cells. ACS Nano. 2014;8:6288–96.
68. Baumgart J, Humbert L, Boulais E, Lachaine R, Lebrun JJ, Meunier M. Off-resonance plasmonic enhanced femtosecond laser optoporation and transfection of cancer cells. Biomaterials. 2012;33:2345–50.
69. Vogel A, Noack J, Hüttman G, Paltauf G. Mechanisms of femtosecond laser nanosurgery of cells and tissues. Appl Phys B Lasers Opt. 2005;81:1015–47.
70. Lyu Z, Zhou F, Liu Q, Xue H, Yu Q, Chen HA. Universal platform for macromolecular Deliveryinto cells using gold nanoparticle layers via the photoporation effect. Adv Funct Mater. 2016;26:5787–95.
71. Katas H, Alpar HO. Development and characterisation of chitosan nanoparticles for siRNA delivery. J Control Release. 2006;115:216–25.
72. Wang L, Wu J, Hu Y, Hu C, Pan Y, Yu Q, Chen H. Using porous magnetic iron oxide nanomaterials as a facile photoporation nanoplatform for macromolecular delivery. J Mater Chem B. 2018;6:4427–36.
73. Zheng Y, Wu Y, Zhou Y, Wu J, Wang X, Qu Y, Wang Y, Zhang Y, Yu Q. Photothermally activated electrospun nanofiber Mats for high-efficiency surface-mediated gene transfection. ACS Appl Mater Interfaces. 2020;12:7905–14.

74. Lu K, Qu Y, Lin Y, Li L, Wu Y, Zou Y, Chang T, Zhang Y, Yu Q, Chen HA. Photothermal nanoplatform with sugar-triggered cleaning ability for high-efficiency intracellular delivery. ACS Appl Mater Interfaces. 2022;14:2618–28.
75. Fouriki A, Dobson J. Nanomagnetic gene transfection for non-viral gene delivery in NIH 3T3 mouse embryonic fibroblasts. Materials. 2013;6:255–64.
76. Okita K, Nakagawa M, Hyenjong H, Ichisaka T, Yamanaka S. Generation of mouse induced pluripotent stem cells without viral vectors. Science. 2008;322:949–53.
77. Yue Y, Jin F, Deng R, Cai J, Chen Y, Lin MC, Kung HF, Wu C. Revisit complexation between DNA and polyethylenimine—effect of uncomplexed chains free in the solution mixture on gene transfection. J Control Release. 2011;155:67–76.
78. Kircheis R, Wightman L, Wagner E. Design and gene delivery activity of modified polyethylenimines. Adv Drug Deliv Rev. 2001;53:341–58.
79. Teo PY, Yang C, Hedrick JL, Engler AC, Coady DJ, Ghaem-Maghami S, George AJ, Yang YY. Hydrophobic modification of low molecular weight polyethylenimine for improved gene transfection. Biomaterials. 2013;34:7971–9.
80. Tian H, Guo Z, Chen J, Lin L, Xia J, Dong X, Chen X. PEI conjugated gold nanoparticles: efficient gene carriers with visible fluorescence. Adv Healthc Mater. 2012;1:337–41.
81. Peng Q, Hu C, Cheng J, Zhong Z, Zhuo R. Influence of disulfide density and molecular weight on disulfide cross-linked polyethylenimine as gene vectors. Bioconjug Chem. 2009;20:340–6.
82. Wu J, Xue H, Lyu Z, Li Z, Qu Y, Xu Y, Wang L, Yu Q, Chen H. Intracellular delivery platform for "recalcitrant" cells: when polymeric carrier marries photoporation. ACS Appl Mater Interfaces. 2017;9:21593–8.
83. Yang J, Feng Y, Zhang L. Biodegradable carrier/gene complexes to mediate the transfection and proliferation of human vascular endothelial cells. Polym Adv Technol. 2015;26:1370–7.
84. Feng Y, Guo M, Liu W, Hao X, Lu W, Ren X, Shi C, Zhang W. Co-self-assembly of cationic microparticles to deliver pEGFP-ZNF580 for promoting the transfection and migration of endothelial cells. Int J Nanomedicine. 2017;12:137–49.
85. Wu MC, Deokar AR, Liao JH, Shih PY, Ling YC. Graphene-based photothermal agent for rapid and effective killing of bacteria. ACS Nano. 2013;7:1281–90.
86. Lin D, Qin T, Wang Y, Sun X, Chen L. Graphene oxide wrapped SERS tags: multifunctional platforms toward optical labeling, photothermal ablation of bacteria, and the monitoring of killing effect. ACS Appl Mater Interfaces. 2014;6:1320–9.
87. Tan SY, Chew SC, Tan SY, Givskov M, Yang L. Emerging frontiers in detection and control of bacterial biofilms. Curr Opin Biotechnol. 2014;26:1–6.
88. Hadjesfandiari N, Yu K, Mei Y, Kizhakkedathu JN. Polymer brush-based approaches for the development of infection-resistant surfaces. J Mater Chem B. 2014;2:4968–78.
89. Wei T, Yu Q, Chen H. Responsive and synergistic antibacterial coatings: fighting against bacteria in a smart and effective way. Adv Healthc Mater. 2019;8:1801381.
90. Zou Y, Zhang Y, Yu Q, Chen H. Dual-function antibacterial surfaces to resist and kill bacteria: painting a picture with two brushes simultaneously. J Mater Sci Technol. 2021;70:24–38.
91. Zou Y, Zhang Y, Yu Q, Chen H. Photothermal bactericidal surfaces: killing bacteria using light instead of biocides. Biomater Sci. 2021;9:10–22.
92. Bassetti M, Merelli M, Temperoni C, Astilean A. New antibiotics for bad bugs: where are we? Ann Clin Microbiol Antimicrob. 2013;12:22.
93. Wilson M. Photolysis of oral bacteria and its potential use in the treatment of caries and periodontal disease. J Appl Bacteriol. 1993;75:299–306.
94. Ray PC, Khan SA, Singh AK, Senapati D, Fan Z. Nanomaterials for targeted detection and photothermal killing of bacteria. Chem Soc Rev. 2012;41:3193–209.
95. Wang Y, Wei T, Qu Y, Zhou Y, Zheng Y, Huang C, Zhang Y, Yu Q, Chen H. Smart, photothermally activated, antibacterial surfaces with thermally triggered bacteria-releasing properties. ACS Appl Mater Interfaces. 2020;12:21283–91.
96. Wang Y, Zou Y, Wu Y, Wei T, Lu K, Li L, Lin Y, Wu Y, Huang C, Zhang Y, Chen H, Yu Q. Universal antifouling and photothermal antibacterial surfaces based on multifunctional

metal–phenolic networks for prevention of biofilm formation. ACS Appl Mater Interfaces. 2021;13:48403–13.
97. Li L, Li G, Wu Y, Lin Y, Qu Y, Wu Y, Lu K, Zou Y, Chen H, Yu Q, Zhang Y. Dual-functional bacterial cellulose modified with phase-transitioned proteins and gold nanorods combining antifouling and photothermal bactericidal properties. J Mater Sci Technol. 2022;110:14–23.
98. Lin Y, Zhang H, Zou Y, Lu K, Li L, Wu Y, Cheng J, Zhang Y, Chen H, Yu Q. Superhydrophobic photothermal coatings based on candle soot for prevention of biofilm formation. J Mater Sci Technol. 2023;132:18–26.
99. Mi L, Jiang S. Integrated antimicrobial and nonfouling zwitterionic polymers. Angew Chem Int Ed. 2014;53:1746–54.
100. Wei T, Tang Z, Yu Q, Chen H. Smart antibacterial surfaces with switchable bacteria-killing and bacteria-releasing capabilities. ACS Appl Mater Interfaces. 2017;9:37511–23.
101. Wei T, Qu Y, Zou Y, Zhang Y, Yu Q. Exploration of smart antibacterial coatings for practical applications. Curr Opin Chem Eng. 2021;34:100727.
102. Yu Q, Chen H. Smart antibacterial surfaces with switchable function to kill and release bacteria. Acta Polym Sin. 2020;51:319–25.
103. Qu Y, Wei T, Zhao J, Jiang S, Yang P, Yu Q, Chen H. Regenerable smart antibacterial surfaces: full removal of killed bacteria via a sequential degradable layer. J Mater Chem B. 2018;6:3946–55.
104. Burda C, Chen X, Narayanan R, El-Sayed MA. Chemistry and properties of nanocrystals of different shapes. Chem Rev. 2005;105:1025–102.
105. Wang D, Ha Y, Gu J, Li Q, Zhang L, Yang P. 2D protein supramolecular nanofilm with exceptionally large area and emergent functions. Adv Mater. 2016;28:7414–23.
106. Gu J, Miao S, Yan Z, Yang P. Multiplex binding of amyloid-like protein nanofilm to different material surfaces. Colloid Interface Sci Commun. 2018;22:42–8.